Astroparticle Physics 30 (2008) 29–38

Contents lists available at ScienceDirect

Astroparticle Physics

journal homepage: www.elsevier.com/locate/astropart

Lock acquisition of the Virgo gravitational wave detector

F. Acernese [g,i], M. Alshourbagy [o,p], P. Amico [m,n], F. Antonucci [s], S. Aoudia [j], K.G. Arun [k], P. Astone [s], S. Avino [g,h], L. Baggio [a], G. Ballardin [b], F. Barone [g,i], L. Barsotti [o,p,aa,*], M. Barsuglia [z], Th.S. Bauer [u], S. Bigotta [o,p], S. Birindelli [o,p], M.A. Bizouard [k], C. Boccara [l], F. Bondu [j], L. Bosi [m], S. Braccini [o], C. Bradaschia [o], A. Brillet [j], V. Brisson [k], D. Buskulic [a], G. Cagnoli [c], E. Calloni [g,h], E. Campagna [c,e], F. Carbognani [b], F. Cavalier [k], R. Cavalieri [b], G. Cella [o], E. Cesarini [c,d], E. Chassande-Mottin [z], S. Chatterji [s], F. Cleva [j], E. Coccia [w,x], C. Corda [o,p], A. Corsi [s], F. Cottone [m,n], J.-P. Coulon [j], E. Cuoco [b], S. D'Antonio [w], A. Dari [m,n], V. Dattilo [b], M. Davier [k], R. De Rosa [g,h], M. Del Prete [o,q], L. Di Fiore [g], A. Di Lieto [o,p], M. Di Paolo Emilio [w,y], A. Di Virgilio [o], M. Evans [b,aa], V. Fafone [w,x], I. Ferrante [o,p], F. Fidecaro [o,p], I. Fiori [b], R. Flaminio [f], J.-D. Fournier [j], S. Frasca [s,t], F. Frasconi [o], L. Gammaitoni [m,n], F. Garufi [g,h], E. Genin [b], A. Gennai [o], A. Giazotto [b,o], V. Granata [a], C. Greverie [j], D. Grosjean [a], G. Guidi [c,e], S. Hamdani [b], S. Hebri [b], H. Heitmann [j], P. Hello [k], D. Huet [b], S. Kreckelbergh [k], P. La Penna [b], M. Laval [j], N. Leroy [k], N. Letendre [a], B. Lopez [b], M. Lorenzini [c,d], V. Loriette [l], G. Losurdo [c], J.-M. Mackowski [f], E. Majorana [s], C.N. Man [j], M. Mantovani [q,p], F. Marchesoni [m,n], F. Marion [a], J. Marque [b], A. Masserot [a], F. Menzinger [b], C. Michel [f], L. Milano [g,h], Y. Minenkov [w], S. Mitra [j], M. Mohan [b], J. Moreau [l], N. Morgado [f], S. Mosca [g,h], B. Mours [a], I. Neri [m,n], F. Nocera [b], G. Pagliaroli [w], C. Palomba [s], F. Paoletti [b,o], S. Pardi [g,h], A. Pasqualetti [b], R. Passaquieti [o,p], D. Passuello [o], F. Piergiovanni [c,e], L. Pinard [f], R. Poggiani [o,p], M. Punturo [m], P. Puppo [s], O. Rabaste [z], P. Rapagnani [s,t], T. Regimbau [j], F. Ricci [s,t], I. Ricciardi [g,h], A. Rocchi [w], L. Rolland [a], R. Romano [g,i], P. Ruggi [b], D. Sentenac [b], S. Solimeno [g,h], B.L. Swinkels [b], R. Terenzi [w], A. Toncelli [o,p], M. Tonelli [o,p], E. Tournefier [a], F. Travasso [m,n], G. Vajente [r,p], J.F.J. van den Brand [u,v], S. van der Putten [u], D. Verkindt [a], F. Vetrano [c,e], A. Viceré [c,e], J.-Y. Vinet [j], H. Vocca [m], M. Yvert [a]

[a] *Laboratoire d'Annecy-le-Vieux de Physique des Particules (LAPP), IN2P3/CNRS, Université de Savoie, Annecy-le-Vieux, France*
[b] *European Gravitational Observatory (EGO), Cascina (Pi), Italy*
[c] *INFN, Sezione di Firenze, Sesto Fiorentino, Italy*
[d] *Università degli Studi di Firenze, Firenze, Italy*
[e] *Università degli Studi di Urbino "Carlo Bo", Urbino, Italy*
[f] *LMA, Villeurbanne, Lyon, France*
[g] *INFN, sezione di Napoli, Italy*
[h] *Università di Napoli "Federico II" Complesso Universitario di Monte S. Angelo, Italy*
[i] *Università di Salerno, Fisciano (Sa), Italy*
[j] *Departement Artemis – Observatoire de la Côte d'Azur, BP 4229 06304 Nice, Cedex 4, France*
[k] *LAL, Univ Paris-Sud, IN2P3/CNRS, Orsay, France*
[l] *ESPCI, Paris, France*
[m] *INFN, Sezione di Perugia, Italy*
[n] *Università di Perugia, Perugia, Italy*
[o] *INFN, Sezione di Pisa, Italy*
[p] *Università di Pisa, Pisa, Italy*
[q] *Università di Siena, Siena, Italy*
[r] *Scuola Normale Superiore, Pisa, Italy*
[s] *INFN, Sezione di Roma, Italy*
[t] *Università "La Sapienza", Roma, Italy*
[u] *National Institute for Subatomic Physics, NL-1009 DB Amsterdam, The Netherlands*
[v] *Vrije Universiteit, NL-1081 HV Amsterdam, The Netherlands*
[w] *INFN, Sezione di Roma Tor Vergata, Roma, Italy*
[x] *Università di Roma Tor Vergata, Roma, Italy*
[y] *Università dell'Aquila, L'Aquila, Italy*
[z] *AstroParticule et Cosmologie (APC), CNRS: UMR7164-IN2P3-Observatoire de Paris-Université Denis Diderot-Paris VII – CEA : DSM/IRFU, France*
[aa] *MIT-LIGO, 185 Albany Street, NW22-295 Cambridge, MA, United States*

* Corresponding author. Present address: MIT-LIGO, 185 Albany Street, NW22-295 Cambridge, MA, United States.
E-mail address: lisabar@ligo.mit.edu (L. Barsotti).

0927-6505/$ - see front matter
doi:10.1016/j.astropartphys.2008.06.005

ARTICLE INFO

Article history:
Received 30 May 2008
Received in revised form 17 June 2008
Accepted 20 June 2008
Available online 28 June 2008

Keywords:
Gravitational wave detectors
Interferometry
Control systems
Lock acquisition

ABSTRACT

The Virgo interferometer for gravitational wave detection has concluded four months of scientific data acquisition in its final optical configuration (a power-recycled interferometer with Fabry-Perot cavities in the arms). The lock acquisition technique developed to bring and keep the Virgo detector on its working point largely proved to be very efficient and robust. In this paper we describe the variable finesse lock acquisition technique and we discuss the performance of the whole locking system.

1. Introduction

The general theory of relativity predicts the existence of *gravitational waves*, perturbations of the space–time metric propagating at the speed of light. Gravitational waves are generated by any mass having a time-varying quadrupole moment. Astrophysical compact objects, such as neutron stars or black holes, are expected to generate detectable signals at different periods of their life: formation, oscillations, collisions, coalescence of binary systems.

Interferometric antennas are designed to measure the slight variation of the difference between the two arm lengths caused by the passage of a gravitational wave. Since the amplitude of the variation is proportional to the arm length, long interferometers are desired for the purpose. However, even considering a few kilometer long arms, the displacements to be detected are of the order of 10^{-18} m, thus making the detection very challenging and requiring very sophisticated technologies.

The idea of using long arm interferometers to detect gravitational waves started to be explored a few decades ago [1], and in the last few years several ground-based laser interferometers have been put into operation: the three LIGO interferometers (2×4 km and 2 km) in the United States [2], the French–Italian (3 km) VIRGO [5], the German–British (600 m) GEO600 [3] and the Japanese (300 m) TAMA300 [4].

1.1. The commissioning of the Virgo detector

As first step in the construction of the detector, the central part of the Virgo interferometer (CITF) was commissioned during the years 2001–2002. The CITF consisted in a power-recycled Michelson interferometer. The main subsystems of Virgo were tested in this simple configuration. In particular, a lock acquisition technique was developed in order to bring and keep the CITF on its working point, by controlling its two longitudinal degrees of freedom [9]. In 2003 the installation of the detector was completed, and the full detector, a power-recycled Michelson interferometer with Fabry Perot cavities in the arms, has been commissioned for several years. Because of the increased complexity of the optical scheme, a new lock acquisition technique had to be developed in order to control all the four longitudinal degrees of freedom of the detector in a robust way. After a few commissioning runs in 2004 and 2005, the first Virgo science run (VSR1) started in 2007, when the interferometer was reliably locked for about four months continuously. We will detail and discuss the Virgo lock acquisition technique.

2. The Virgo detector

The Virgo detector is based on a laser interferometer (ITF) with 3 km long arms (see Fig. 1 for ITF optical layout). In order to amplify the phase shift produced by a variation of the laser beam optical path length, each arm is replaced by a Fabry-Perot cavity having a finesse of 50. Statistical fluctuations of the number of photons detected at the anti-symmetric (ASY) port are the fundamental source of noise in the high frequency range (above a few hundred Hz). A performance improvement is achievable by increasing the number of photons injected into the arms[1] and then maximizing the power circulating inside the ITF. To this purpose the ASY port is tuned onto the dark fringe to minimize the transmitted power. All the light reflected back to the laser source can be then re-injected into the ITF by properly placing an additional mirror (the power recycling mirror, PR) between the laser source and the ITF. In this way, the total amount of power impinging upon the beam-splitter (BS) is increased by about a factor 40. The input beam is produced by a laser Nd:Yag ($\lambda = 1064$ nm) with a power of 20 W. It is stabilized in frequency and position both by active controls and by passive filtering through a suspended triangular 144 m long cavity, the input mode-cleaner (IMC). With the present laser beam set-up configuration only a power of about 8 W arrives to the PR mirror to be used within the ITF so that the total amount of power impinging upon the BS mirror is about 320 W [6]. The gravitational wave signal is detected at the ASY port.

The Virgo main optics are fused silica cylinders, with a diameter of 35 cm and mass of 20 kg. They are suspended in vacuum from a multi-stages pendulum which reduces the transmission of the seismic noise at the payload level by more than 10 orders of magnitude in all the degrees of freedom, starting from a few Hz. This pendulum chain, together with a mechanical three legs elastic structure, based on the working principle of an inverted pendulum (IP), represent the most original part of the experimental apparatus called Superattenuator (SA) [7]. The introduction of the IP has two main reasons: it is a pre-isolation stage along the laser beam direction starting from a very low frequency (about 40 mHz) and it is a very soft mechanical structure from which the whole SA can be easily moved by means of an active control. The SA, indeed, has been designed to confine the mechanical resonance modes of the structure in the low frequency region.

Below 4 Hz, the seismic isolation is performed by an active control system, which operates at three levels. The first action is performed on top of the chain where the suspension point is controlled by three positioning sensors and three accelerometers. This feedback control is called Inertial Damping and is able to reduce the residual motion of the suspension point down to a few tenths of micron r.m.s. At the bottom of the chain each mirror is

[1] The number N of detected photons follows Poissonian statistics, with fluctuation proportional to $\sqrt{N}$. On the other hand, the signal produced by the passage of the gravitational wave is proportional to N, so that the signal to noise ratio (SNR) is proportional to $\sqrt{N}$.

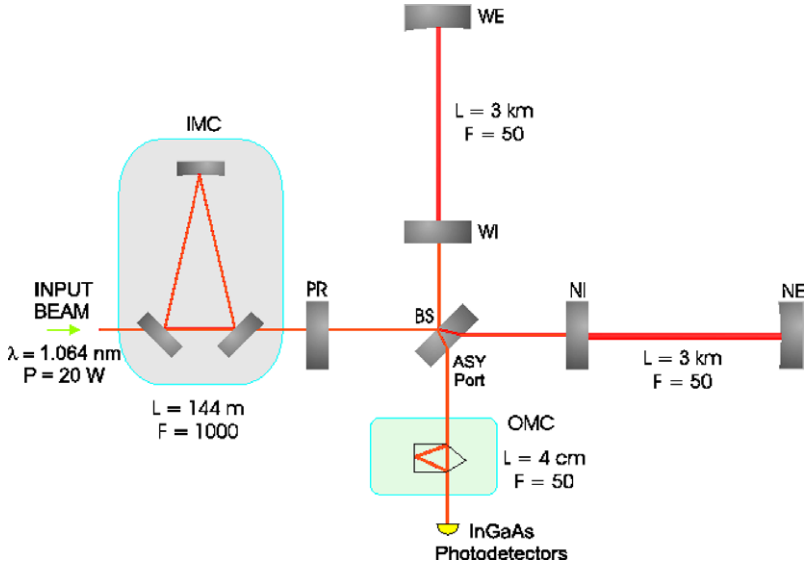

Fig. 1. Virgo layout.

hung to an intermediate mass, the *Marionette*, by means of two thin steel wires in a cradle configuration. An additional mechanical element, the *Reference Mass*, is suspended from the Marionette and surrounds the mirror. The Marionette itself is suspended from the last stage of the SA. The second action consists in acting on the marionette from the last stage of the SA, and the third one in acting on the mirror position from the Reference Mass. A detailed description of the control system was given in [8].

The best sensitivity of the detector is achieved when the interferometer is controlled on its operating point:

- the laser light resonant in the optical cavities;
- the anti-symmetric port set on the dark fringe.

These conditions translate into fixed relationships between the laser light wavelength and four independent lengths of the interferometer (see Fig. 2):

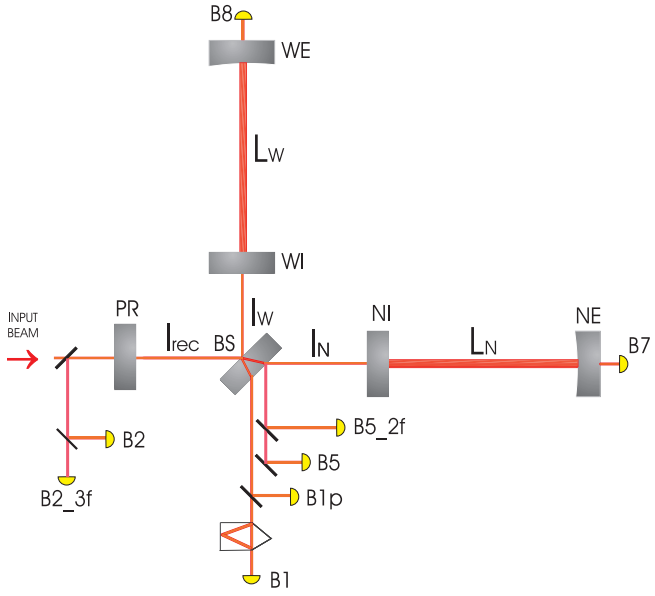

Fig. 2. Optical scheme of the Virgo ITF. In the schema are indicated the main optics: the power recycling mirror (PR), the beam-splitter mirror (BS), input and end mirrors of the North and West arms (NI, WI, NE and WE). The names of the photodiodes placed at the different output ports of the ITF are also indicated.

- the length of the recycling cavity (PRCL), $l_{rec} + \frac{l_N + l_W}{2}$;
- the differential length of the short Michelson arms (MICH), $l_N - l_W$;
- the common (CARM) and the differential (DARM) length of the two long arms, $L_N + L_W$ and $L_N - L_W$.

Even if the seismic attenuation performance obtained with the SA is very good, the mirror residual longitudinal motion (1 μm) is about 50 times larger than the Fabry-Perot cavity resonance width (20 nm), and a million times larger than the requirement for reaching shot-noise limited sensitivity (1 pm). An active longitudinal control system able to achieve the required resonance conditions has been implemented. Moreover, preventing that intensity noise dominates over shot-noise, the allowed deviation from the working point at the ASY port represents a six order of magnitude more stringent parameter to be considered. An active global longitudinal control system is therefore needed in order to bring and to keep the low frequency swinging mirrors in their working position with sufficient accuracy [10].

3. The longitudinal control system

The longitudinal control scheme adopted in Virgo is based on a standard Pound–Drever–Hall technique [11,12]. By applying a frontal modulation, the carrier beam is phase modulated with an electro-optic modulator at a radio frequency before entering the IMC. The modulation frequency ($f = 6.26$ MHz for Virgo) is chosen so that carrier and sidebands fields behave differently inside the ITF:

- the carrier fields resonate inside the recycling cavity and in the Fabry-Perot arms, and interfere destructively (dark fringe) at the ASY port;
- the recycling cavity is also on resonance for the sum of the sidebands, which are almost totally reflected by the arm cavities (where they do not resonate).

Photodiodes placed at the main output ports of the ITF detect the beating between carrier and sidebands. By demodulation at the modulation frequency and its multiples (in Virgo signals are demodulated at twice, $2f$, and three times, $3f$, the modulation frequency), signals sensitive to interferometer length variations can be extracted. A set of signals has to be chosen in order to build a

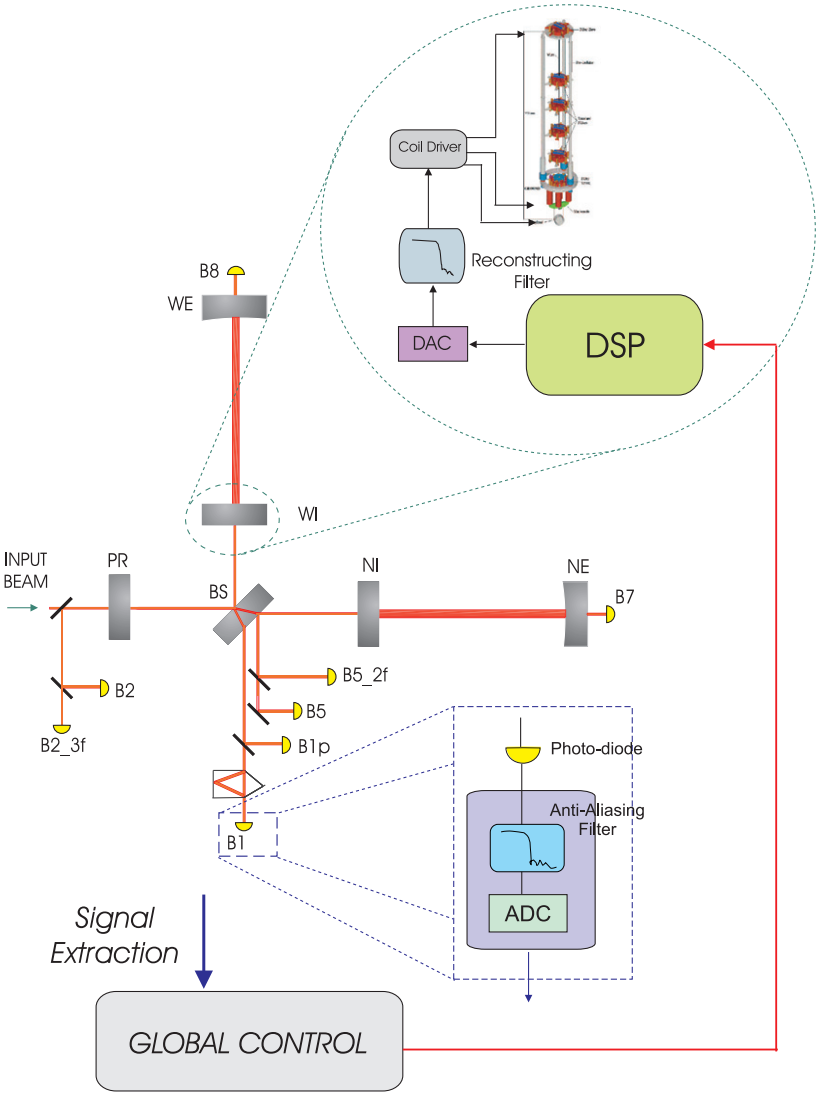

Fig. 3. Longitudinal control chain. Signals extracted from the ITF by photodiodes are sent to the Global Control, which combines them to compute corrections, which are sent to the DSP of the involved suspensions.

sensing matrix which reconstructs the four lengths of the ITF. Error signals for each degree of freedom are then filtered to produce correction signals which are fed-back to the corresponding mirrors in order to keep them at the desired working point. The control chain is fully digital, as summarized in Fig. 3. Signals detected at the output ports of the ITF are sampled at 20 kHz by 16 bit analog-to-digital converters (ADCs) and sent to the global control system [13], which computes the correction signals to be applied to the mirrors. Digital corrections are sent to digital signal processors (DSP) running on each suspension. The DSP's filter them to produce the signals which drive the coil–magnet actuators.

The computational time delay accumulated in the control chain sets constraints on the bandwidth of the longitudinal loops. It can be estimated in the following way [14]:

- Signals extracted from the ITF are sampled at a frequency $f_s = 20$ kHz and averaged every two times. This adds a delay $\Delta t_1 = 1/f_s = 50$ μs;
- the Locking process runs at 10 kHz. By considering at least two sampling periods to process the signals and send them to the suspension crates, the accumulated time delay is $\Delta t_2 = 200$ μs;
- suspension DSP's run at 10 kHz. One sampling period is needed to process the data, causing a time delay $\Delta t_3 = 100$ μs;

The estimated total delay Δt is at least:

$$\Delta t = \Delta t_1 + \Delta t_2 + \Delta t_3 = 350\ \mu s$$

The corresponding phase delay at a given frequency f is:

$$\Delta\phi = 2\pi f \Delta t$$

It results that the unity gain frequency of the longitudinal control loops cannot be larger than about 100 Hz.

4. The variable finesse locking technique

The Pound–Drever–Hall technique provides signals sensitive to interferometer length variations only in the steady-state regime of the ITF, that is around its operating point. No useful error signal can be extracted far from the operating point. Therefore a suitable locking strategy should be developed starting from the initial uncontrolled state of the ITF, where mirrors are freely swinging, and reaching the final locked state where the four lengths of the ITF are kept controlled on their operating point. The problem is usually referred to as lock acquisition. The lock acquisition procedure of a power-recycled ITF was systematically addressed in other experiments, such as LIGO [17] and TAMA [19]. In both the cases it is

based on a statistical approach, where the control loops are engaged every time the ITF passes through the relative resonance conditions. Since LIGO and Virgo have a quite similar optical setup, the successful strategy adopted in the LIGO detectors has been in particular studied.[2]

With a sequential procedure the four independent lengths of the interferometer are locked and the optical sensing matrix is changed in a dynamic way compensating the field variation during the lock acquisition process.[3] Starting from the uncontrolled condition the ITF is then locked on its operating point in a few minutes by adopting a three steps sequence as follows:

- In the first step the sidebands enter in resonance in the recycling cavity (not resonant in the arms), the carrier is on the anti-resonance for the recycling cavity and not resonant in the arms;
- in the second step the carrier becomes resonant in one arm, on the bright fringe in the recycling cavity. The sidebands remain in the same condition as the previous step;
- in the final step the carrier becomes resonant in both arms and in the recycling cavity, corresponding to the working point of the ITF.

Since the working point is reached through a sequence of unstable states, locking parameters needed to reach the final state (demodulation phases and optical gains of the error signals) can only be extrapolate from easier stable optical configurations [16]. This means that they are not experimentally measurable.

Together with the difficulty in estimating the locking parameters, the multi-step technique, which was initially tested, showed other weak points when applied to Virgo. The Virgo suspensions are much softer than LIGO ones: they attenuate better all frequencies above 2–3 Hz, but the remaining mirror motion at low frequencies is larger. By applying the multi-step technique, mirrors are typically shaken for at least a couple of minutes before the lock acquisition, by making the lock acquisition itself more challenging. Moreover, because of additional delays in the digital control system (see Section 3), unity gain frequencies of the digital loops can not be set much higher than 100 Hz (about a factor two bigger in LIGO). This makes the frequency noise contamination coupled into the CARM degree of freedom and the lock acquisition procedure becomes more difficult.

In order to overcome these problems, a different lock acquisition technique was developed and successfully applied to the Virgo interferometer [18]. The main idea is to start the locking sequence with an optical configuration easy to lock, so as to control all the longitudinal degrees of freedom, and then move from this initial state to the final one in an adiabatic way. The complexity in controlling a recycled ITF arises from the presence of the PR mirror, which couples the fields inside the ITF. By reducing the recycling gain, all the ITF degrees of freedom are weakly coupled and independently controllable, making the control scheme much easier. A low recycling gain configuration can be obtained by initially locking the ITF at mid-fringe, that is the point in which the power transmitted to the dark port is half of the power in the recycling cavity. In this way, a large fraction of light escapes through the anti-symmetric port and the power build-up inside the recycling cavity is extremely low. From this stable state, in which all the degrees of freedom are already controlled, the ITF can be adiabatically brought to the operating point, by moving the Michelson

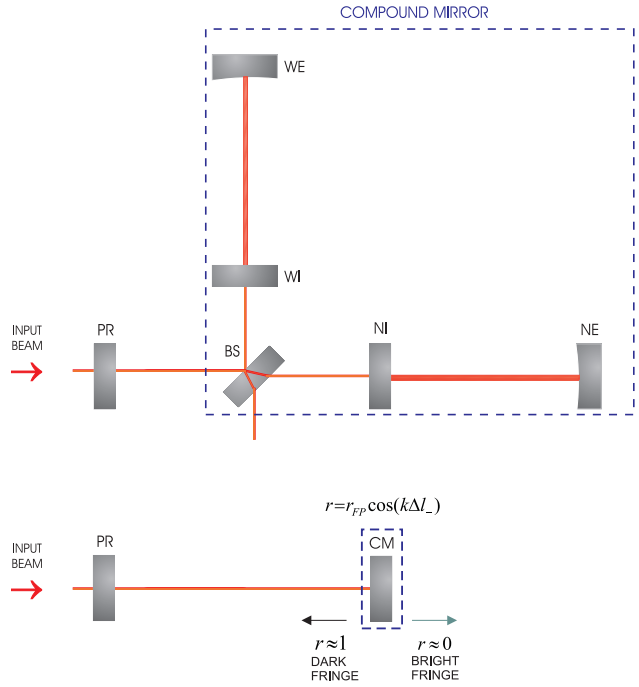

Fig. 4. The ITF seen as a variable finesse cavity formed by the PR mirror and the compound mirror. The reflectivity on the compound mirror depends on the detuning of the ITF from the dark fringe condition: it is maximum when the ITF is on the dark fringe, while it vanishes on the bright fringe, when all the power is transmitted.

from mid-fringe to the dark fringe. Because the finesse of the recycling cavity changes during the locking sequence, this locking technique is usually referred to as variable finesse (see Fig. 4).

The advantage of this strategy is that the interferometer pass through stable states in which different degrees of freedom are kept locked. In this situation the locking parameters are experimentally measurable with the locking procedure in progress. As a consequence of it the tuning of the control system becomes simpler and faster. Moreover, this allows the engagement of the analog frequency servo even when the interferometer is not yet on its working point. This aspect is particularly relevant in reducing the frequency noise which would contaminate the control signals used for lock acquisition. A global control of the ITF angular degrees of freedom can be engaged during the locking sequence as well, improving the mirror alignment conditions and making the locking itself simpler.

The locking procedure starts with the PR mirror slightly misaligned by some μrads, in order to further decrease the power stored inside the recycling cavity.[4] Since all the degrees of freedom are almost decoupled in this state, the two arms can be independently locked using the photodiodes placed in transmission of the two arms (B7 and B8, see Fig. 2). The Michelson is kept controlled at mid-fringe (see Fig. 5). This is done by adding an offset in the anti-symmetric port DC signal[5] and sending the correction to the BS mirror. The signal is normalized so that an offset of 0.5 corresponds to the mid-fringe lock. The small quantity of light reflected by the ITF is used to control the recycling cavity length, by means of the reflected 3f-demodulated signal ($B2\_3f$). The use of

[2] Lock acquisition in TAMA is simplified by the fact that the recycling gain is about a factor 10 lower than in Virgo and in LIGO, which makes the arm cavities much less coupled.

[3] From the uncontrolled state to the fully controlled state, in fact, the resonant power inside the LIGO ITF changes by more than three orders of magnitude, and the response of the involved error signals varies accordingly (see [15]).

[4] It is worth mentioning that the initial misalignment of the PR mirror is not a fundamental requirement, and the lock can be successfully achieved in this first step even keeping it in its pre-aligned position. However, experiments showed that the initial misalignment of the PR mirror considerably speeds up the locking procedure.

[5] A standard Pound–Drever–Hall signal could not be used, as it would be outside of its linear range with the Michelson at mid-fringe.

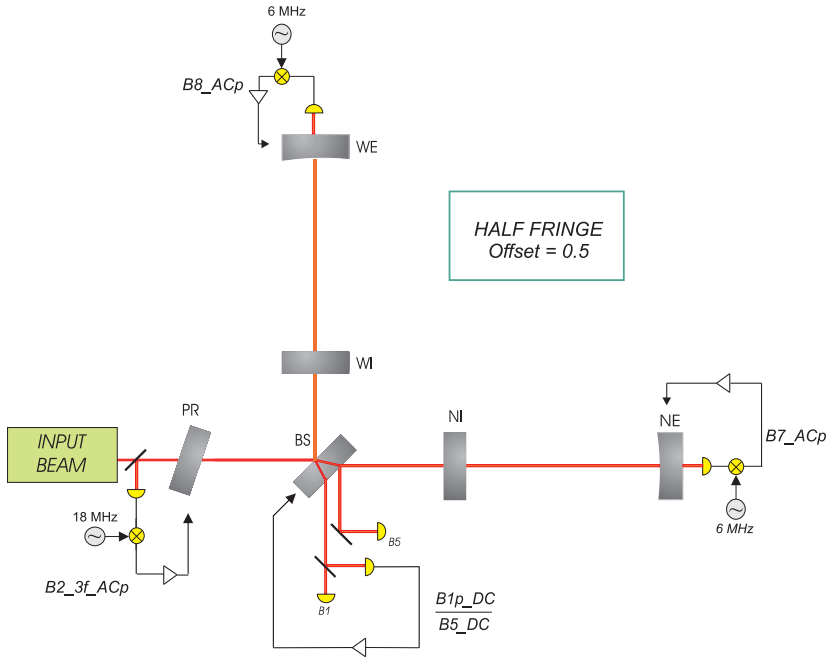

Fig. 5. Locking scheme in the first step of the lock acquisition sequence: the two long cavities are independently locked by the end demodulated signals, the Michelson is controlled by a DC error signal (B1p_DC/B5_DC). The PR mirror is kept slightly misaligned, and the small quantity of light reflected back by the ITF is used to control the recycling cavity length by the 3*f*-demodulated signal (B2_3*f*).

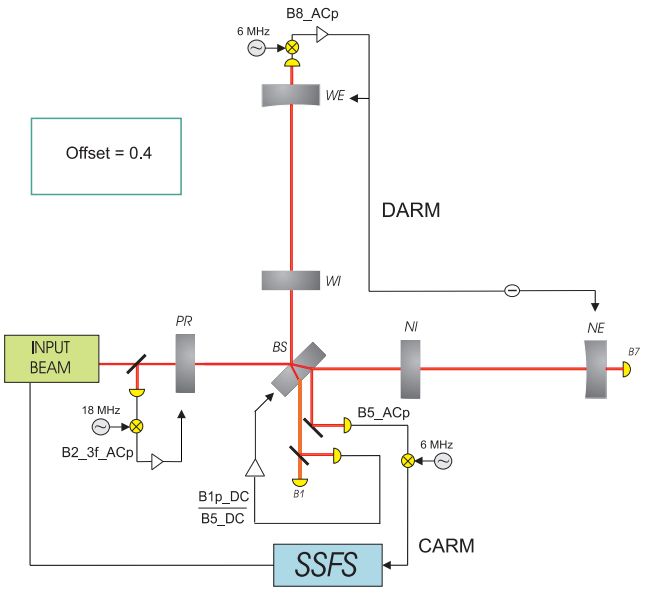

Fig. 6. Evolution of the locking scheme: when the fringe offset is reduced, a differential and common control of the arms is needed to take into account the increasing coupling between the two cavities. *B8_ACp* is applied for the differential control, the frequency stabilization servo is engaged for the common control.

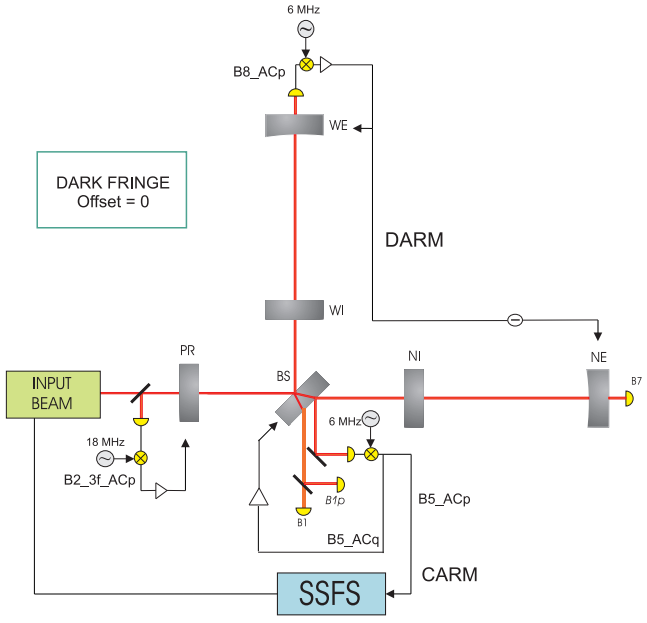

Fig. 7. Evolution of the locking scheme: close to the dark fringe the offset in the DC signal is removed and it is replaced by the demodulated signal *B5_ACq*.

the 3*f*-demodulated signal has been successfully tested in the TAMA control scheme [19] and it has the advantage of being less sensitive to the optical parameters of the ITF than the standard *f*-demodulated signal. The stability of amplitude and sign of the PRCL reconstructed length even with strong variations of the optical parameters allows the same feedback topology to be maintained for the whole locking sequence.

With an initial pre-alignment of the mirrors within half of μrad, this stable configuration can be usually reached in a few seconds, preventing mirror excitations. From this starting condition the PR is realigned maintaining the Michelson controlled at mid-fringe and keeping the recycling gain low. In order to increase the recycling gain, the Michelson has to be brought on the dark fringe: this is done adiabatically, decreasing the offset in the Michelson error signal. At the same time the control scheme evolves to take into account the increasing coupling among the different degrees of freedom. The signals extracted from the photodiodes B7 and B8 can be used to independently control the cavities only when the ITF is far from the dark fringe. When approaching the dark fringe the common and differential control (CARM and DARM) have to be

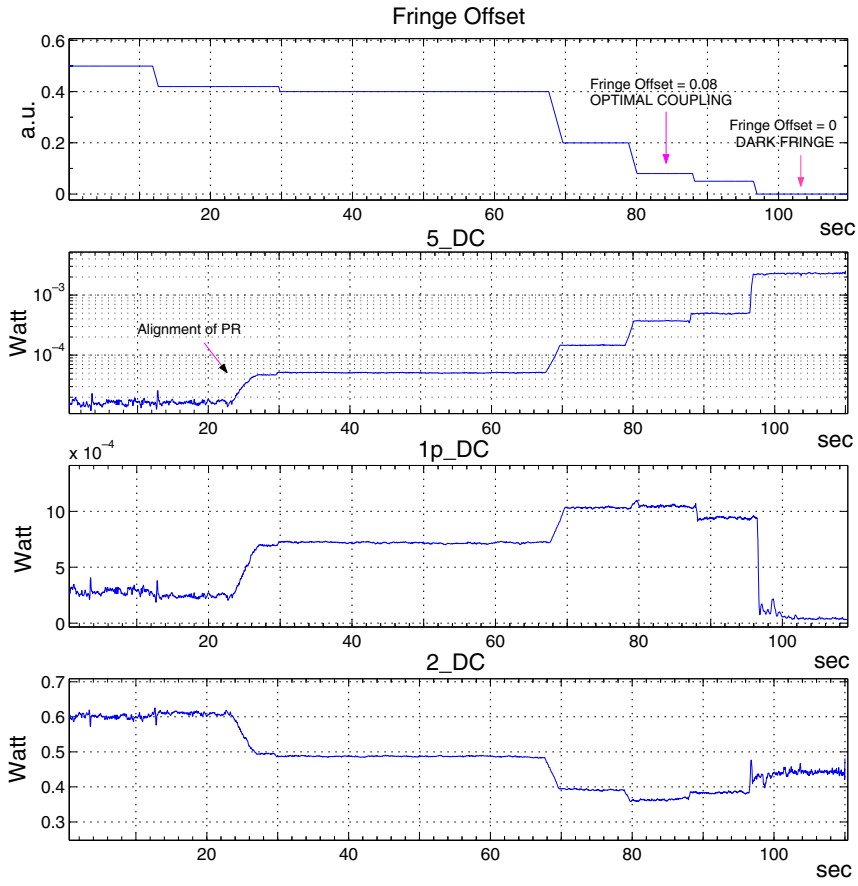

Fig. 8. Trend of the power stored inside the recycling cavity (*B5_DC*), the power at the dark port (*B1p_DC*) and power reflected by the ITF (*B2_DC*) during a lock acquisition sequence. The first plot shows the value of the fringe offset: its value of 0.08 corresponds at the optimal coupling for the recycling cavity (no mode matched light is reflected from the cavity), 0 is the dark fringe condition.

activated to keep the lock, since both cavities become strongly coupled.

While DARM is controlled by B8, a frequency stabilization servo is engaged to control CARM (see Fig. 6). A high bandwidth analog loop, around 20 kHz, is adopted, so that the contamination by this degree of freedom is greatly reduced. Since the laser beam entering the ITF is already prestabilized in frequency, this further reduction of the frequency noise is referred in Virgo as the second stage of frequency stabilization (SSFS [20]).

The final step of the locking sequence (see Fig. 7) consists of switching from a DC signal to a demodulated signal to control the Michelson length. Eventually the offset in the Michelson error signal is removed: the ITF goes on to the dark fringe and the recycling cavity gain increases up to the maximum value. The DARM control is moved from the end photodiode signal to the anti-symmetric port signal extracted before the OMC (B1p), mainly for noise reduction purposes.[6] The PRCL degree of freedom remains stably controlled by the reflected 3*f*-demodulated signal during the entire lock acquisition sequence.

The behavior of the powers inside the ITF during a full locking sequence is shown in Fig. 8.

4.1. The control filters

Several digital filters are used during the locking sequence. The lock of the ITF at mid-fringe is acquired by means of a simple derivative filter with a very low unity frequency gain for all the degrees of freedom. Once the ITF is locked in a stable way, the DC gain is increased, reducing the residual motion of the mirrors. In Fig. 9 the control filters for MICH and PRCL degrees of freedom are plotted.

The first step of the sequence concerns the independent locking of the long cavities that is obtained applying a derivative filter with an integrator up to 10 Hz. As soon as the independent control of the two cavities is active, DARM is kept controlled by using the same filter with unitary gain frequency at about 100 Hz (see Fig. 10). The measured DARM locking accuracy is of the order of 10^{-13} m. The CARM error signal is fed-back to the laser by means of a large bandwidth (about 20 kHz) analog integrative filter. During the lock acquisition sequence, several gain stages are implemented compensating for the increasing of the CARM error signal optical gain.

5. Noise reduction

Once the interferometer is locked on the dark fringe the main goal becomes the noise reduction to reach the best detector sensitivity. This is done passing through several steps devoted to isolate different noise sources and giving relevant contributions. The first low-noise transition is performed putting on resonance the OMC and then using the signal downward it (B1) to control the DARM degree of freedom. This signal has a better signal to noise ratio with respect to B1p, used in the first locking phase and picked-up upward the OMC. The control noise spoiling B1 is then reduced by applying more aggressive filtering of the MICH and PRCL signals,

[6] The transmission of the end mirrors is quite low, about 50 ppm. Due to low power, the signal to noise ratio of the transmitted power is quite poor.

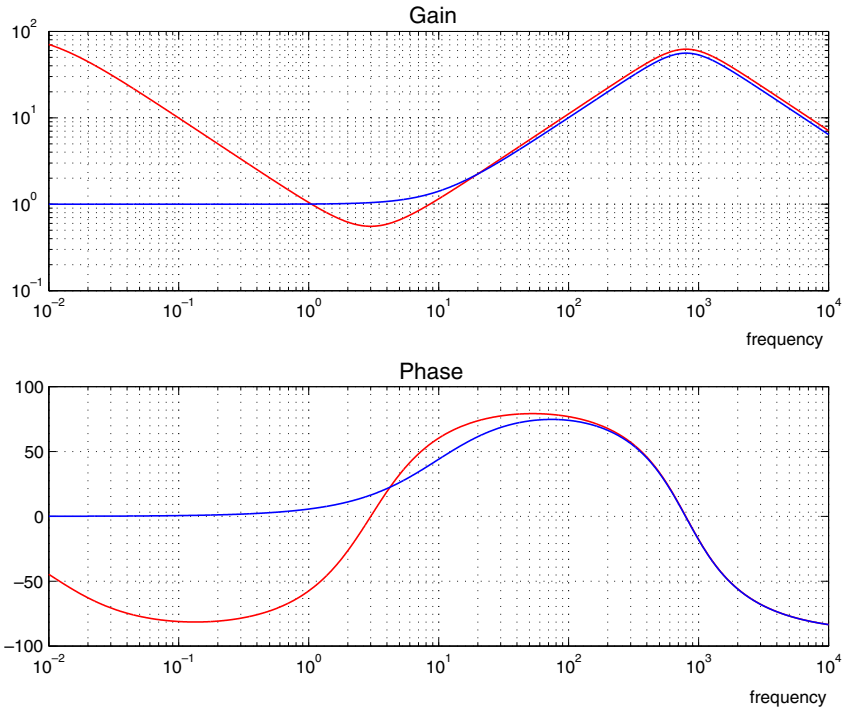

Fig. 9. Control filters for MICH and PRCL: the simpler one (in blue) is used to acquire the lock at mid-fringe. Once lock is acquired, a new filter (in red) with 100 times higher gain at 10 mHz is engaged. (For interpretation of the references in colour in this figure legend, the reader is referred to the web version of this article.)

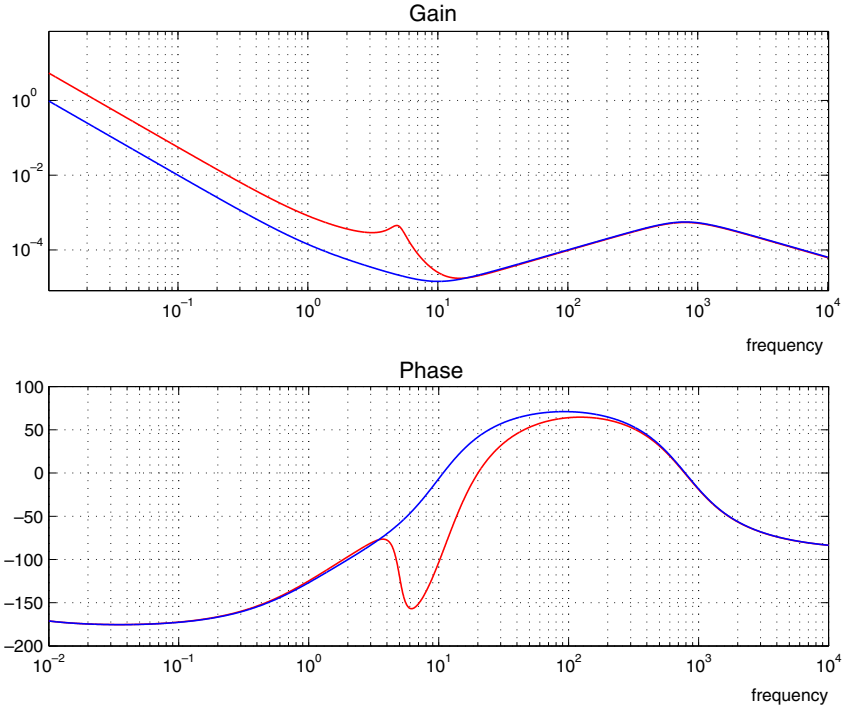

Fig. 10. Control filters for DARM: the blue one is applied in the first steps of the sequence; when the fringe offset is decreased up to 0.2, the red one is switched on, in order to further increase the DC gain. (For interpretation of the references in colour in this figure legend, the reader is referred to the web version of this article.)

with cut-off frequencies of 50 and 200 Hz respectively and unity gain frequency around 15 Hz for MICH and 35 Hz for PRCL. Finally, the MICH correction signal cancelation is enabled to further reduce the contamination of the dark fringe signal from the MICH control noise. This cancelation is provided by driving the end mirrors differentially (essentially the DARM drive) with a small signal derived from the MICH control signal such that the transfer function from the MICH error point to B1 is minimized. A less noisy signal for controlling PRCL is also adopted, moving the control from the 3f to the f demodulated signal extracted at the reflection port of the

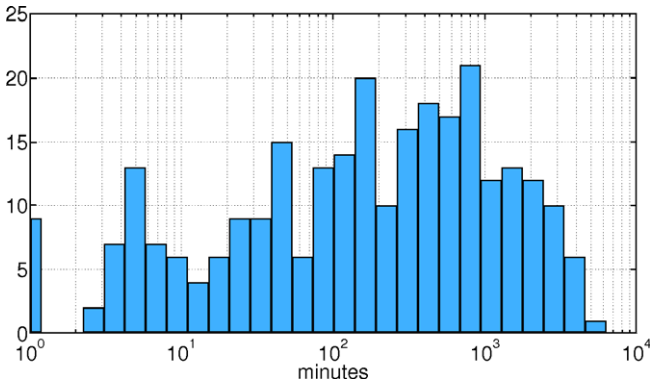

Fig. 11. Distribution of lock duration in VSR1.

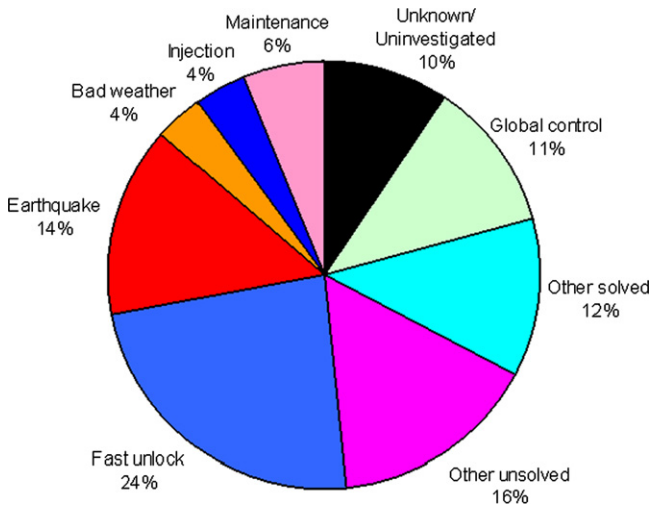

Fig. 12. Main causes of unlock of the ITF from the final locked state in VSR1.

ITF (B2). A cancelation of the PRCL correction signal, similar to the MICH one, is enabled as well.

The hierarchical control of the Superattenuator is then engaged. It is based on the possibility to apply some correction signals to the suspension upper stages removing the feedback action from the mirror. The low frequency component (below 10 Hz) is sent to the marionette, reducing the re-injected noise at this frequency to the mirror level. As a consequence of it, the re-allocation of control force reduces the dynamic range requirement of the reaction mass coil driver, which in turn allows for a transition to lower noise electronics. The transition is made in three steps: re-allocation of force to the marionette, switch of DAC channels to use low-noise path in the coil-drivers while zeroing the signal passing through the high-noise path, opening of the relay connecting the high-noise drive to the reaction mass coils.

Once all the noise reduction operations are performed, the final science mode state is reached and the ITF is ready for data acquisition. The full locking procedure, from the uncontrolled state to science mode, requires that about four hundred of commands are sent to the real-time processors of the main sub-systems. A fully automated locking procedure was developed in order to manage all these operations. In a sequence of different steps, the final science mode state can be reached in not more than 5 min, typically without human intervention.

6. Results

At the beginning of the year 2006, after the lock acquisition procedures was tested with a laser power of 700 mW, an additional Faraday isolation system was installed between the IMC and the recycling mirror. The laser power entering into the ITF was set to 8 W. The increased power improved the interferometer sensitivity at high frequency, but it had the consequence of creating more thermal lensing than was expected on the basis of absorption measurements of the mirror coatings. Developing a stable control system, in the presence of thermal lensing and the absence of thermal compensation, turned out to be very challenging.

Although the variable finesse approach remained unchanged in its basic lines, important improvements have been developed at the control level to guarantee stable servos during the thermal transient. Demodulating lines injected at various points in the system provides a constant monitor of many of the locking parameters, such as RF demodulation phases and unity gain frequencies of the loops. Automatic adjustment of the loop gains were also implemented in order to guarantee stability during lock acquisition and to keep the parameters well tuned afterwards. However, the detector low-noise performance was achievable only by waiting for the end of the thermal transient. This had the obvious drawback of significantly increasing the time from lock loss to stable

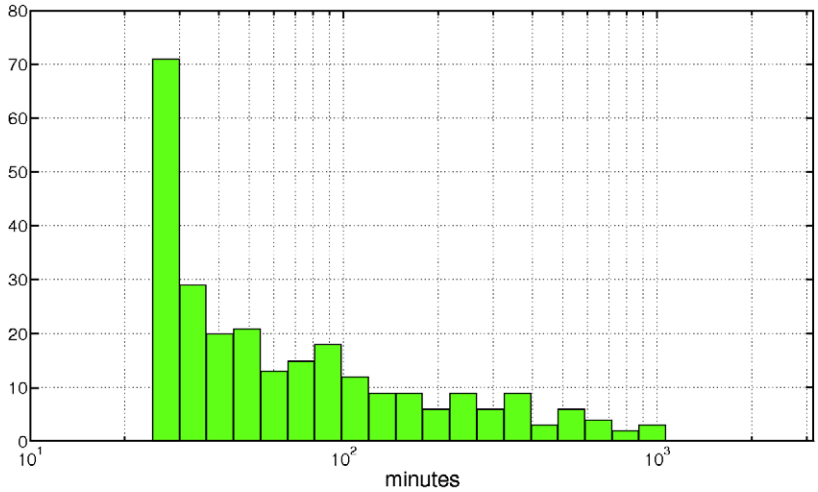

Fig. 13. Distribution of the elapsed time between a lock loss and the following relock of the ITF in VSR1. The time spent for both commissioning activities and detector maintenance is included in the distribution (with a typical elapsed time of 4 h).

operation: about 30 min from the initial uncontrolled state of the ITF to the final science mode state.

6.1. The first Virgo science run

On 18th May 2007 the first Virgo science run (VSR1) started and lasted for four and a half months. Remarkable results have been obtained in terms of reliability and robustness of the lock acquisition procedure, which contributed to achieve a duty cycle in the final locked state of about 84% (slightly less, about 81%, is the duty cycle in science mode). The longest consecutive lock lasted 94 h (almost four days) and there were about 20 locking periods longer than 40 h. Totally, the ITF was locked in the final state for more than 2700 h, with an average lock duration of 10 h. Fig. 11 shows the distribution of lock durations.

From science mode, the ITF unlocked 229 times, with an average of 1.7 unlocks per day. The main causes of unlocks are shown in Fig. 12. About 25% of the unlocks were due to failures in the injection system (fast unlocks of the IMC control loops). The recovery time associated with this problem consisted mainly of the time required to relock the ITF. This problem was addressed during the run itself, and fixed with a better characterization and tuning of the IMC control loop. The other main causes of unlocks have been crashes of the global control server and earthquakes.

The total down time of the ITF was about 540 h. About 150 h (28%) were spent for detector maintenance (four consecutive hours per week) and planned commissioning activity (a few hours per week in the second part of the run). Fig. 13 shows the distribution of the elapsed time between each lock loss and the following relock. The mean value is about 2 h, the longest down time of the ITF (due to a failure of the air conditioning system in the laser laboratory) is about 17 h. In 27% of the cases the time spent to relock the ITF was about 30 min, meaning that no extra time beyond that required by the standard locking procedure was needed. A recovery time of 2 h was sufficient to relock the ITF in 77% of the cases.

7. Conclusion

The first Virgo science run ended on 1st October 2007. After four and a half months of continuous data acquisition, the variable finesse technique adopted to lock the ITF was demonstrated to be very robust and reliable. A very high duty cycle (about 84%) with the ITF locked in its final state has been obtained as well as a large number of continuous locking periods longer than 40 h.

References

[1] R. Weiss, MIT Quarterly Progress Report, Research Laboratory of Electronics, 105, 54, 1972.
[2] D. Sigg, (for the LIGO Science Collaboration), Status of the LIGO detectors, Class. Quantum Grav. 23 (2006) S51–S56.
[3] H. Lück et al., Status of the GEO600 detector, Class. Quantum Grav. 23 (2006) S71–S78.
[4] K. Arai, for the TAMA collaboration, Current efforts on the TAMA300 detector Amaldi, in: 6th Proceedings, 2005.
[5] F. Acernese et al., The status of Virgo, Class. Quantum Grav. 23 (2006) S63–S69.
[6] F. Acernese et al., Measurement of the optical parameters of the Virgo interferometer, Appl. Opt. 46 (2007) 3466–3484.
[7] S. Braccini et al., Measurement of the seismic attenuation performance of the VIRGO Superattenuator, Astro. Phys. 23 (2005) 557–565.
[8] F. Acernese et al., First locking of the Virgo central area interferometer with suspension hierarchical control, Astro. Phys. 20 (2004) 629–640.
[9] F. Acernese et al., Lock acquisition of the central interferometer of the gravitational wave detector Virgo, Astro. Phys. 21 (2004) S465–S477.
[10] L. Barsotti, The control of the Virgo interferometer for gravitational wave detection, PhD Thesis, Pisa University, 2006.
[11] R.V. Pound, Electronic frequency stabilization of microwave oscillators, Rev. Sci. Instrum. 17 (1946) 490–505.
[12] R.W.P. Drever et al., Laser phase and frequency stabilization using an optical resonator, Appl. Phys. B: Photophys. Laser Chem. 31 (1983) 97–105.
[13] F. Cavalier et al., The global control of the Virgo experiment, Nucl. Instrum. Methods Phys. Res. 550 (2005) 467–489.
[14] M. Barsuglia, L. Di Fiore, G. Giordano, D. Passuello, Definition of band-width and slope of the servo-loop for SA control, Virgo internal note, VIR-NOT-NAP-1390-143.
[15] P. Fritschel et al., Readout and control of a power-recycled interferometric gravitational wave antenna, LIGO note, LIGO-P000008-A-D, 2000.
[16] M. Evans, Lock acquisition in resonant optical interferometers, PhD Thesis, CALTECH, 2001.
[17] M. Evans et al., Lock acquisition of a gravitational-wave interferometer, Opt. Lett. 27 (8) (2002). April 15.
[18] F. Acernese et al., The variable finesse locking technique, Class Quant. Grav. 23 (2006) S85–S89.
[19] K. Arai, and TAMA collaboration, Sensing and controls for power-recycling of TAMA300, Class Quant. Grav. 19 (7) (2002) 1843–1848.
[20] F. Bondu, Design of the last stage of frequency stabilisation and laser frequency noise requirements, Virgo internal note VIR-NOT-OCA-1390-227, 2002.